Electronic Supplementary Information

Room Temperature Switching of a Neutral Molecular Iron(II) Complex

Bernhard Schäfer[a], Cyril Rajnák[a], Ivan Šalitroš[a,e], Olaf Fuhr[a], David Klar[b], Carolin Schmitz-Antoniak[b], Heiko Wende[b], Eugen Weschke[c] and Mario Ruben[a,d]*

Table of Contents

[a] *Institute of Nanotechnology, Karlsruhe Institute of Technology (KIT), Postfach 3640, 76021 Karlsruhe, Germany. E-mail: mario.ruben @kit.edu*

[b] *Faculty of Physics and Center for Nanointegration Duisburg-Essen (CENIDE), University of Duisburg-Essen, Lotharstraße 1, 47048 Duisburg, Germany.*

[c] *Helmholtz-Zentrum Berlin für Materialien und Energie (HZB), Albert-Einstein-Str. 15, 12489, Berlin, Germany*

[d] *Institute de Physique et Chimie des Matériaux de Strasbourg (IPCMS), CNRS-Université de Strasbourg, 23, rue du Loess, BP 43, 67034 Strasbourg cedex 2, France*

[e] *Institute of Inorganic Chemistry, Technology and Materials, Faculty of Chemical and Food Technology, Slovak University of Technology, Bratislava, 812 37, Slovak Republic*

1. Synthesis and structural identification

General

Purchased chemicals and solvents ($Fe^{II}(BF_4)_2 \cdot 6H_2O$, methanol, *n*-hexane, ethyl acetate, and dichloromethane) were used as received. DMF was dried over CaH_2 under argon and distilled. 2-(1H-pyrazol-1-yl)pyridine was prepared as described elsewhere.[S1] Elemental analysis on carbon, hydrogen, and nitrogen was carried out by Vario Micro Cube. FT-IR spectra were measured in KBr pellets (Magna FTIR 750, Nicolet) in the region of 4000–400 cm^{-1}. ^{1}H and ^{13}C NMR spectroscopic data were recorded on a Bruker Ultrashield plus 500 spectrometer with solvent-proton as internal standard. Electrospray ionization time of flight (ESI TOF) mass spectrometric analytical data were acquired on a micrOTOF -Q II Bruker spectrometer.

Synthesis

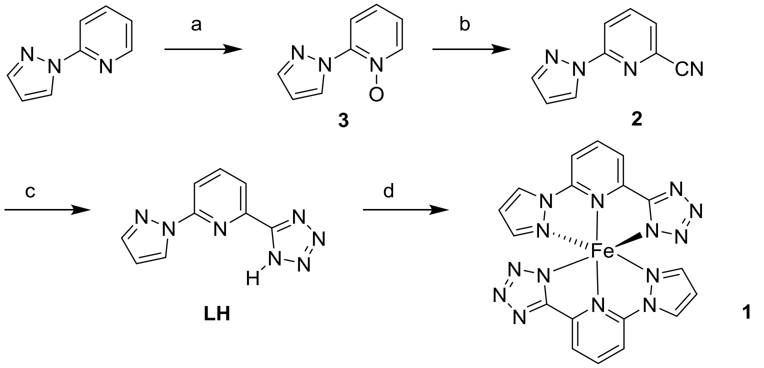

Scheme S1: Synthesis of **1**, a) H_2O_2 and CF_3COOH, b) TMS-CN, benzoyl chloride, CH_2Cl_2 c) NaN_3, NH_4Cl, and DMF (110°C), d) CH_2Cl_2, MeOH, KO*t*Bu, $Fe(H_2O)_6(BF_4)_2$

Synthesis of [Fe(**L**)$_2$], (**1**)

2-(1*H*-pyrazol-1-yl)-6-(1*H*-tetrazol-5-yl)pyridine (0.226 g, 1.06 mmol, 2 eq.) was dissolved in CH_2Cl_2 (40 mL) and MeOH (13 mL) and degassed with argon. KO*t*Bu (0.119 g, 1.06 mmol, 2 eq.) was added and stirred for 30 minutes before $Fe(H_2O)_6(BF_4)_2$ (0.179 g, 0.53 mmol, 1 eq) was added to this solution and allowed to react overnight. The solution was filtered. The corresponding Fe complex was crystallized by slow evaporation of the solvent over the course of a few days (0.188 g, 74%). Elemental analysis: calc. for **1**$\cdot 0.9CH_2Cl_2$ ($C_{18.9}H_{15.8}FeN_{14}$) C, 40.78; H, 2.5; N, 35.23; found C, 39.93; H, 2.99; N, 35.84. Melting point 333-335 °C. ^{1}H NMR (500 MHz, CD_2Cl_2/MeOD 1:1) δ(ppm) 41.69, 37.24, 32.33, 28.49, 22.62, 10.02. UV-VIS (CH_2Cl_2/CH_3OH, 3:1): λ_{max}/nm ($\varepsilon/10^4 M^{-1}cm^{-1}$)=260(4.1), 306(3.1), 449(0.45). FT-IR (KBr) ν/cm^{-1}

3087(w), 1619(m), 1578(m), 1532(m), 1484(s), 1405(m), 1350(m), 1175(m), 1039(m), 806(w), 784(w), 761(w). ESI-TOF MS (CH_2Cl_2/CH_3OH): *m*/*z* = 503.03 $[M+Na]^+$.

Ligand preparation.

Synthesis of 2-(1H-Pyrazol-1-yl)6-(1H-tetrazol-5-yl)pyridine (**LH**)

6-(1H-pyrazol-1-yl)pyridine-2-carbonitrile (0.426g, 2.5 mmol, 1 eq.), NaN_3 (0.366 g, 5.63 mmol, 2.25 eq.), and NH_4Cl (0.301 g, 5.63 mmol, 2.25 eq.) was suspended in freshly distilled dry DMF (5 mL) and heated at 100°C under an atmosphere of N_2 overnight. The reaction was poured into 40 mL of water and 1M HCl was used to acidify to the pH of about 3-4. The white precipitate was filtered, washed with water (5 x 3 mL) and dried at vacuo (0.451 g, 84%). Elemental analysis: calc. for **LH**·0.1 $H_2O(C_9H_{7.2}N_7O_{0.1})$ C, 50.28; H, 3.38; N, 45.60; found C, 50.27; H, 3.61; N, 45.54. Melting point 256–258 °C. ^1H NMR (500 MHz, C_2D_6OS) δ(ppm) 9.04 (d, *J*= 2.25 Hz, 1H), 8.23 (t, *J*= 8 Hz,1H), 8.10 (m, *J*= 0.63 Hz, 2H), 7.89 (d, *J*= 1.25 Hz, 1H) 6.68 (q, *J*= 1.5Hz, 1H). ^{13}C NMR (125 MHz, d6-DMSO) δ(ppm) 154.27, 150.79, 142.87, 141.96, 141.60, 128.02, 119.77, 113.73, 108.59. UV-VIS (CH_2Cl_2/MeOH; 3:1): λ_{max}/nm $(\varepsilon/10^4M^{-1}cm^{-1})$=261(1.44),269(1.45), 311(1.15). FT-IR (KBr) ν/cm^{-1} = 3102(w),1605(m), 1577(m), 1558(m), 1524(m), 1470(s), 1395(s), 1205(w), 1177(w), 1053(s), 939(m), 812(m), 774(w), 750(s). ESI-TOF MS (CH_2Cl_2/CH_3OH): *m*/*z* = 236.05 $[M+Na]^+$.

Synthesis of 6-(1H-pyrazol-1-yl)pyridine-2-carbonitrile (**2**)

To an ice-cooled solution of **3** (0.644 g, 4 mmol) and trimethylsilylcyanide (2 mL, 16 mmol) in ca. 12 mL of CH_2Cl_2 (freshly distilled of CaH_2) under N_2 was carefully added benzoyl chloride (2 eq. ,0.93 mL 8 mmol). After stirring for 23 h at room temperature, 20 mL of a 1 M Na_2CO_3 was carefully added to the chilled reaction mixture (effervescence of the solution occurs). The mixture was extracted with dichloromehane (30 mL x 3 times) and the combined organic phase was dried over $MgSO_4$. The purification by column chromatography was carried out on SiO_2 using *n*-hexan and CH_2Cl_2. Yield (0.44g, 64%). Elemental analysis: calc. for **2**·0.1 H_2O ($C_9H_{6.2}N_4O_{0.1}$) C, 62.86; H, 3.63; N, 32.58; found C, 63.08; H, 3.26; N, 32.11. Melting point 115–117 °C. ^1H NMR (500 MHz, $CDCl_3$) δ(ppm) 8.57 (d, *J*= 2.5 Hz, 1H), 8.24 (d, *J*= 8.5 Hz, 1H), 7.94 (t, *J*= 8 Hz, 1H), 7.76 (d, *J*= 0.5 Hz, 1H), 7.57 (d, *J*=7.5Hz, 1H), 6.51 (t, *J*=2Hz, 1H). ^{13}C NMR (125 MHz, $CDCl_3$) δ(ppm) 152.17, 143.13, 139.70, 131.73, 127.61, 125.81, 116.74, 116.34, 108.66. UV-VIS (CH_2Cl_2): λ_{max}/nm $(\varepsilon/10^4M^{-1}cm^{-1})$=263(1.5), 296(0.75). FT-IR (KBr): ν/cm^{-1} = 3086(w), 2234(w), 1593(s), 1576(m), 1524(m), 1464(s), 1395(s), 1207(m), 948(m), 811(s), 768(s). ESI-TOF MS (CH_2Cl_2): *m*/*z* = 171.05 $[M+H]^+$.

Synthesis 2-(1*H*-pyrazol-1-yl)pyridine 1-oxide (**3**) (adapted from a procedure for 2,2'-bpy)[S2]

2-(1H-Pyrazol-1-yl)pyridine (22g) was dissolved in CF_3COOH (50mL). H_2O_2 (30%, 20mL) was carefully added to this solution. The reaction was heated with an oil-bath at 60°C. After 17h another 10 mL of H_2O_2 was added and left to react overnight. The reaction was stopped, allowed to cool to rt, poured on ice. The pH was carefully ajusted to a value of 10 with 8M KOH. The product was extracted with dichloromethane (4 x 30 mL). The organic layer was dried over Na_2SO_4 and the filtered. The solvent was removed by reduced pressure. The compound was purified by column chromatography on silica (eluent CH_2Cl_2 /MeOH). Yield 70%. Elemental analysis: calc. for **3** ($C_8H_7N_3O$) C, 59.62; H, 4.38; N, 26.07; found C, 59.54; H, 4.32; N, 25.74. Melting point 80-82 °C. ^{1}H NMR (500 MHz, $CDCl_3$) δ(ppm) 9.37 (d, *J*=2.5 Hz,1H), 8.31 (d, *J*=7.0 Hz, 1H), 8.13 (d, *J*=2.0 Hz, 1H), 7.77 (s, 1H), 7.39 (t, *J*=7.75 Hz, 1H), 7.17 (t, *J*=3.75 Hz, 1H), 6.49 (t, *J*= 2.0Hz, 1H). ^{13}C NMR (125 MHz, $CDCl_3$) δ(ppm) 144.63, 142.22, 140.76, 132.99, 127.23, 122.01, 120.02, 107.41. UV-VIS (CH_2Cl_2): λ_{max}/nm ($\varepsilon/10^{4}M^{-1}cm^{-1}$)=255(0.3), 287(0.1). FT-IR (KBr): ν/cm^{-1} = 3169(w), 1610(w), 1562(w), 1517(w), 1498(s), 1407(m), 1291(m), 1235(m), 1045(m), 832(m), 763(s). ESI-TOF MS (CH_2Cl_2): *m*/*z* = 162.06 $[M+H]^{+}$.

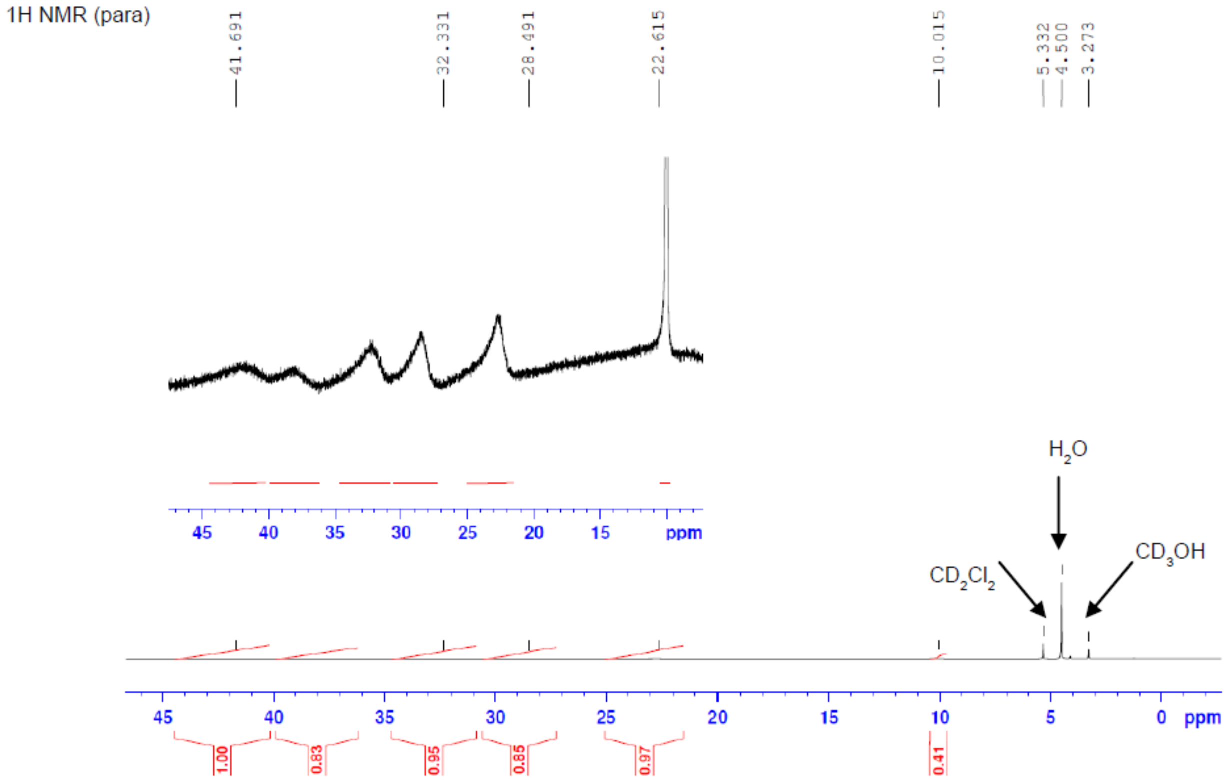

Figure S1. ^{1}H NMR (para) of **1** in CD_2Cl_2/CD_3OH (1:1).

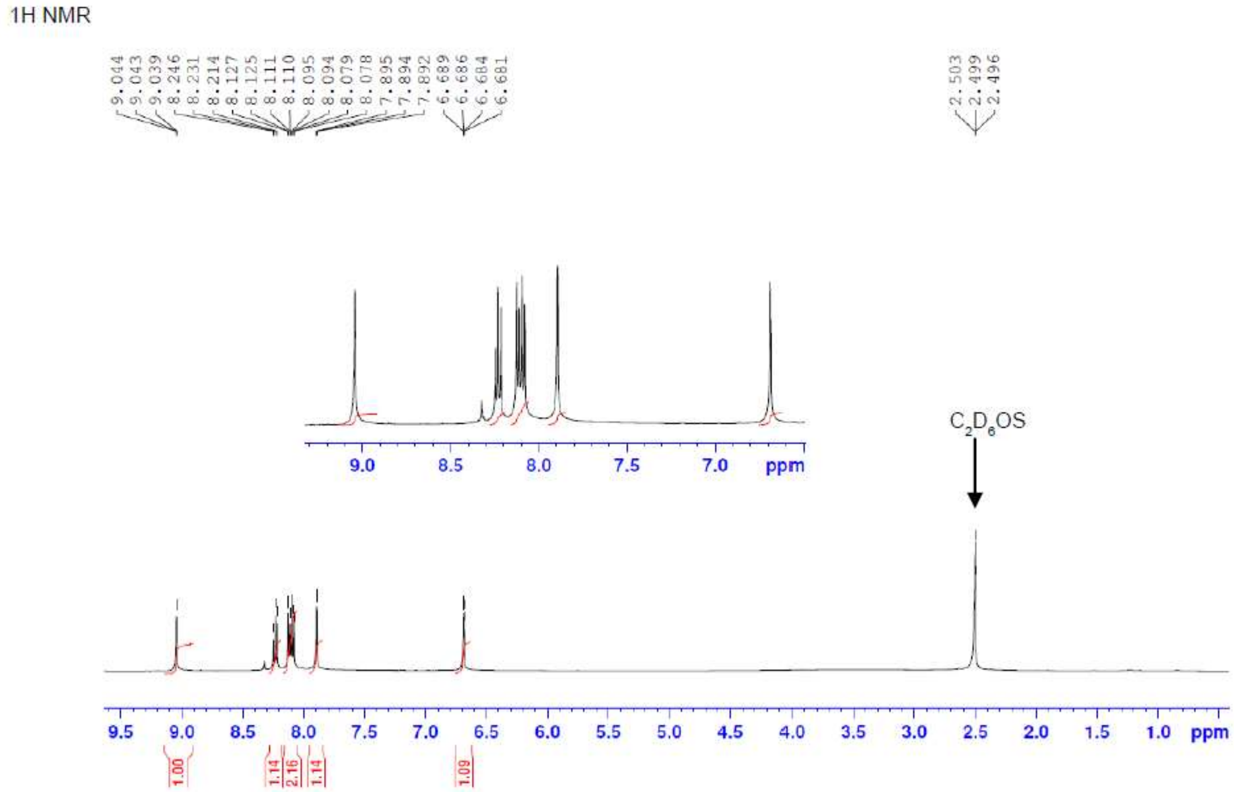

Figure S2. ^{1}H NMR of **LH** in C_2D_6OS.

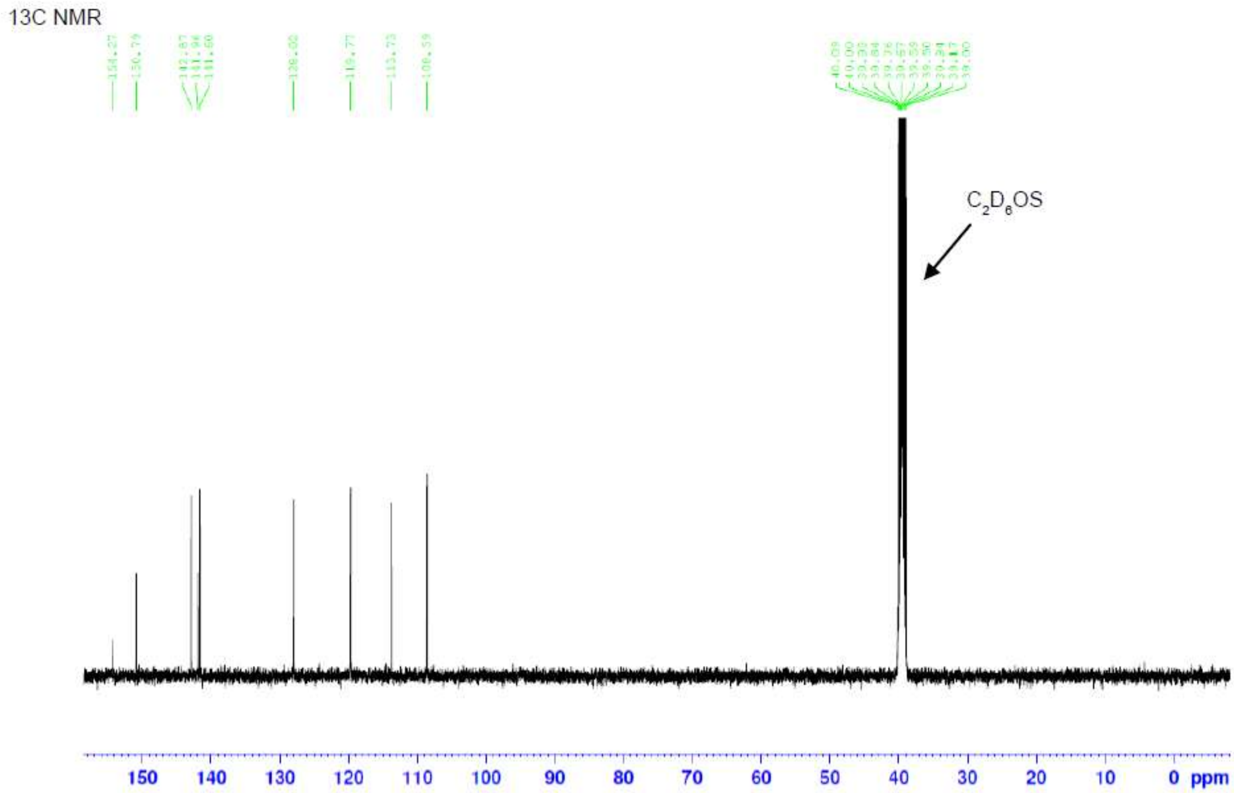

Figure S3. ^{13}C NMR of **LH** in C_2D_6OS.

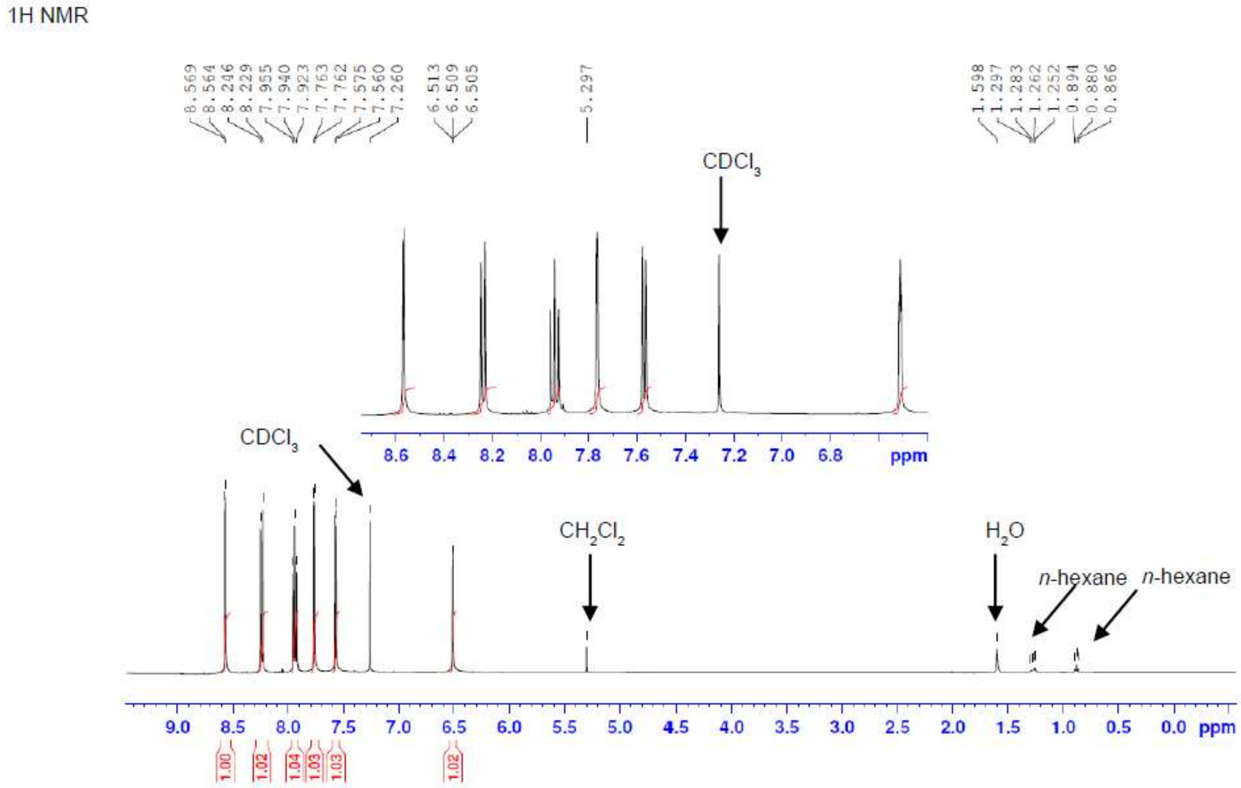

Figure S4. ^{1}H NMR of **2** in $CDCl_3$.

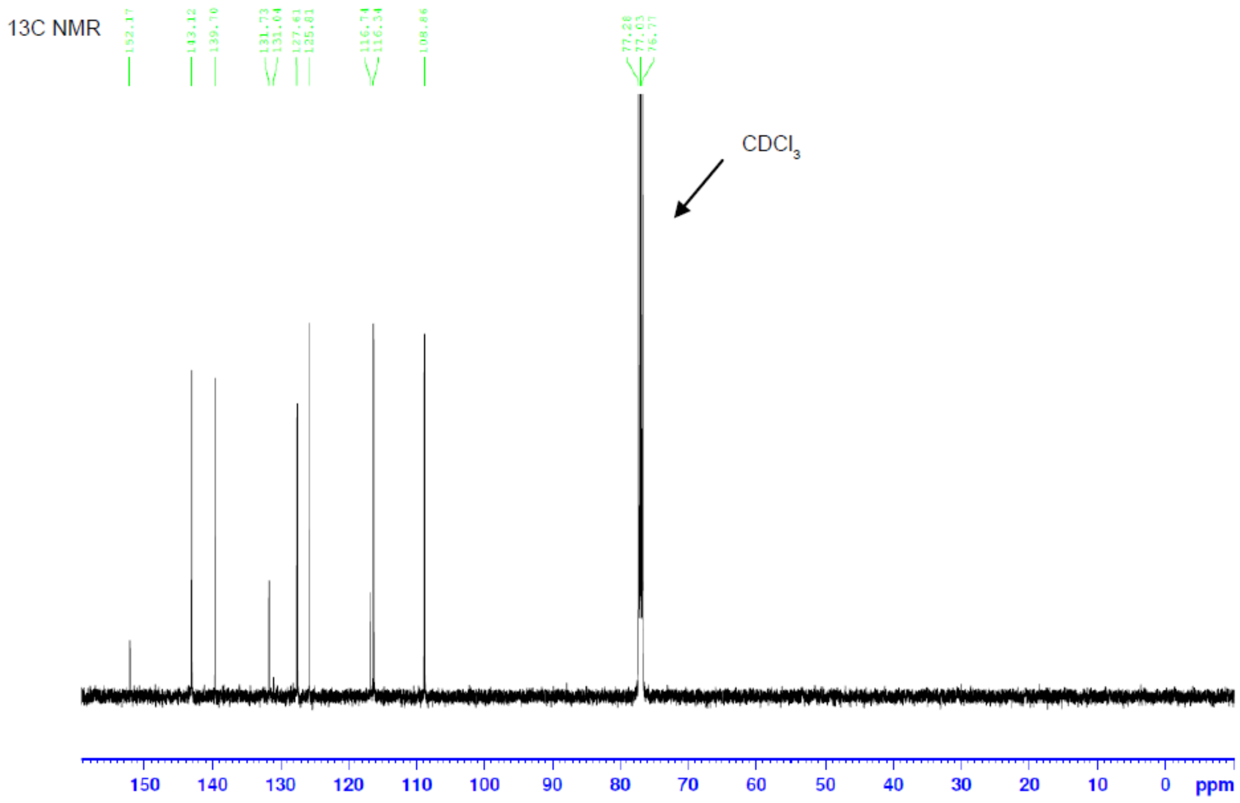

Figure S5. ^{13}C NMR of **2** in $CDCl_3$.

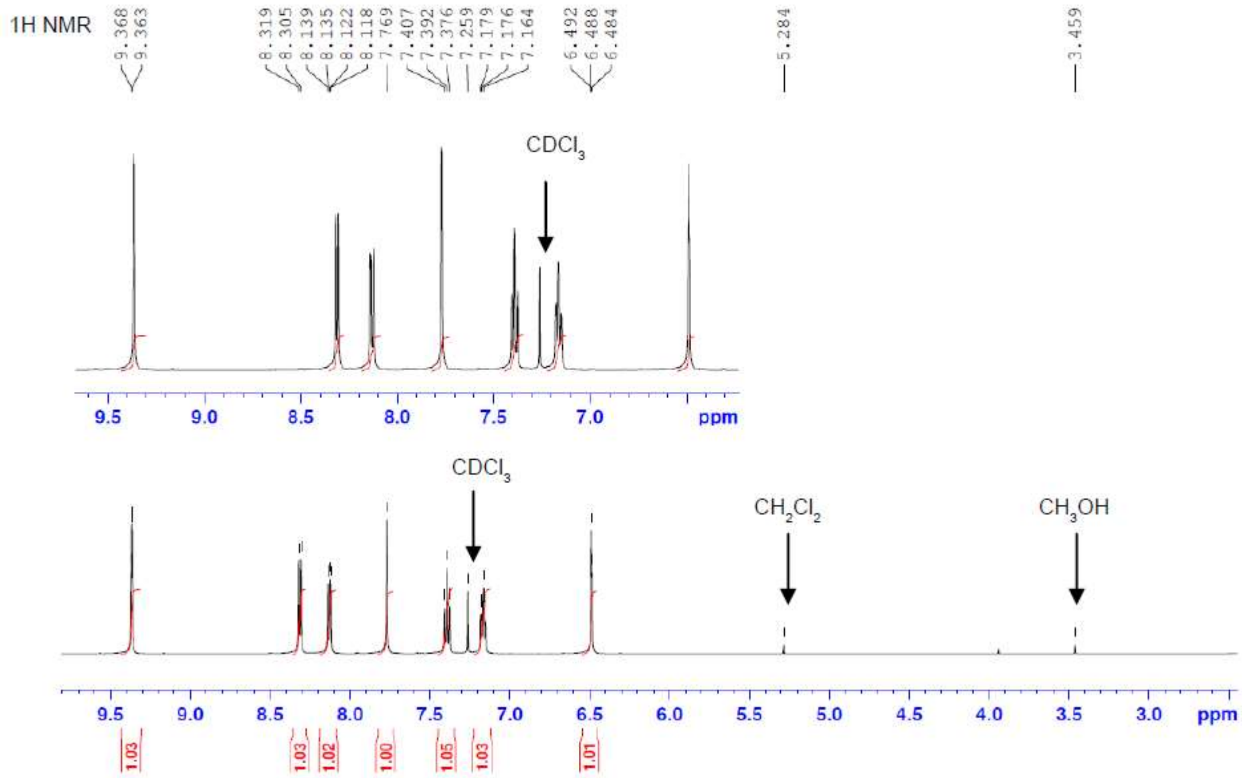

Figure S6. ^{1}H NMR of **3** in $CDCl_3$.

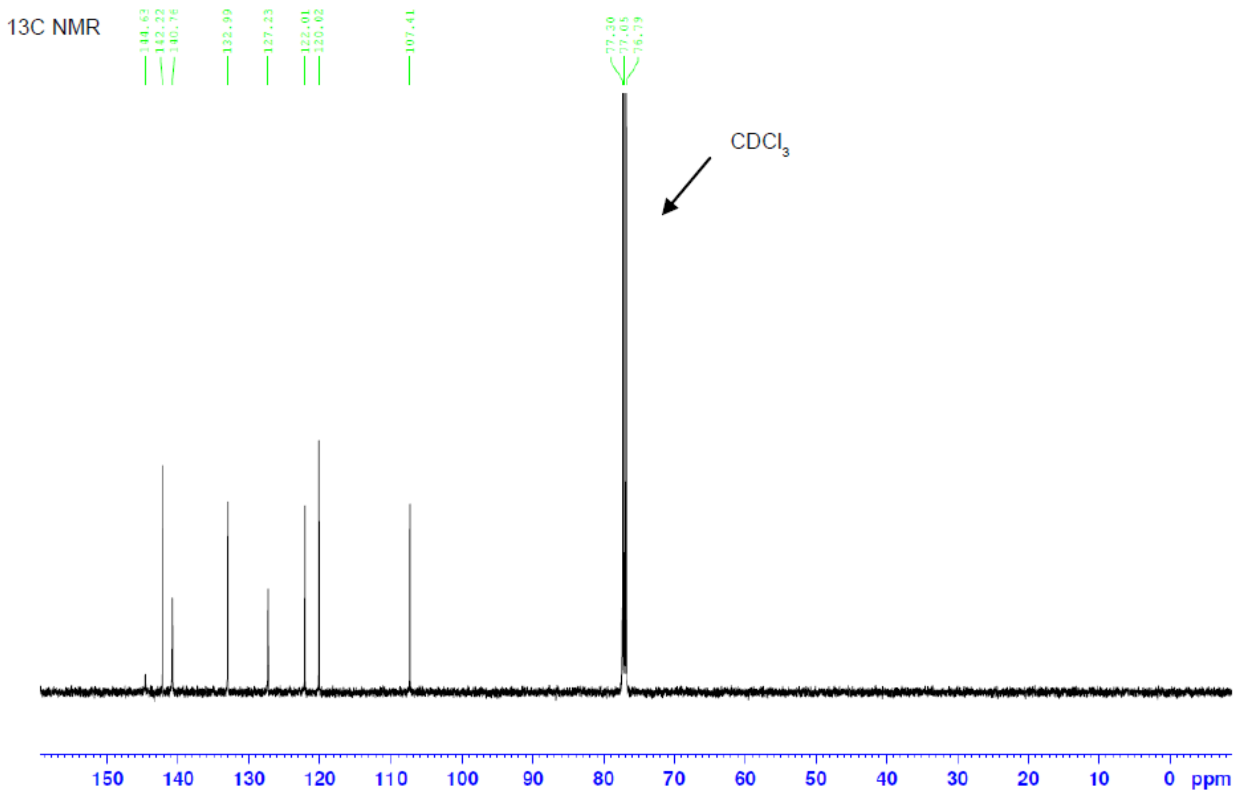

Figure S7. ^{13}C NMR of **3** in $CDCl_3$.

2. Magnetic susceptibility measurements

All herein reported magnetic measurements were performed on a SQUID magnetometer (Quantum Design, model MPMS-XL-5 or MPMS-XL-7). In all cases, the temperature dependence of the magnetic moment was recorded at B = 0.1 T as an external magnetic field. The temperature sweeping rate was 1 K min^{-1} and it was the same for cooling and heating modes. Gelatine capsules as sample containers for the measurement in the temperature range 5–370 K were used. The very small diamagnetic contribution of the gelatine capsule and high temperature sample holder had a negligible contribution to the overall magnetisation, which was dominated by the sample. The diamagnetic corrections of the molar magnetic susceptibilities were applied using Pascal's constants.[S3] The photomagnetic measurements were performed by using a diode-pumped solid-state laser (DPSS) Kvant (λ= 532 nm, 300 mW) coupled through an optical fibre to the cavity of the MPMS SQUID and the power at the sample surface was adjusted to 10 mW cm^{-2}. For the photomagnetic experiments, the mixture of sample and low temperature grease was filled into small quartz glass jar and mounted into the sample holder. The weight of compound **1** (ca. 0.33 mg) was obtained by weighting in the quartz glass jar. After slowly cooling to 10 K, the sample, now in the low spin state, was irradiated and the change in magnetisation followed. When the saturation point had been reached (after ca. 70 min), the light was switched off, the temperature was increased at a rate of 0.3 K min^{-1}, and the magnetisation was measured at 1 K intervals. T(LIESST) was determined from the minimum of the $\partial(\chi_M T)/\partial T$ *vs* *T* curve for the relaxation process. Since we have observed that the quartz glass jar filled with low temperature grease only (in the absence of sample) exhibits very small paramagnetic signal rather stable with temperature (ca. 1.0×10^{-5} cm^3), all magnetic data were corrected for this background value and then processed into χT product function.

3. Crystallographic data of **1**

Single crystal X-ray diffraction data were collected on a STOE IPDS II diffractometer with graphite monochromated Mo-Kα radiation (0.71073 Å). The structures were solved by direct methods (SHELX-97). Refinement was performed with anisotropic temperature factors for all non-hydrogen atoms (disordered atoms were refined isotropically).[S4]

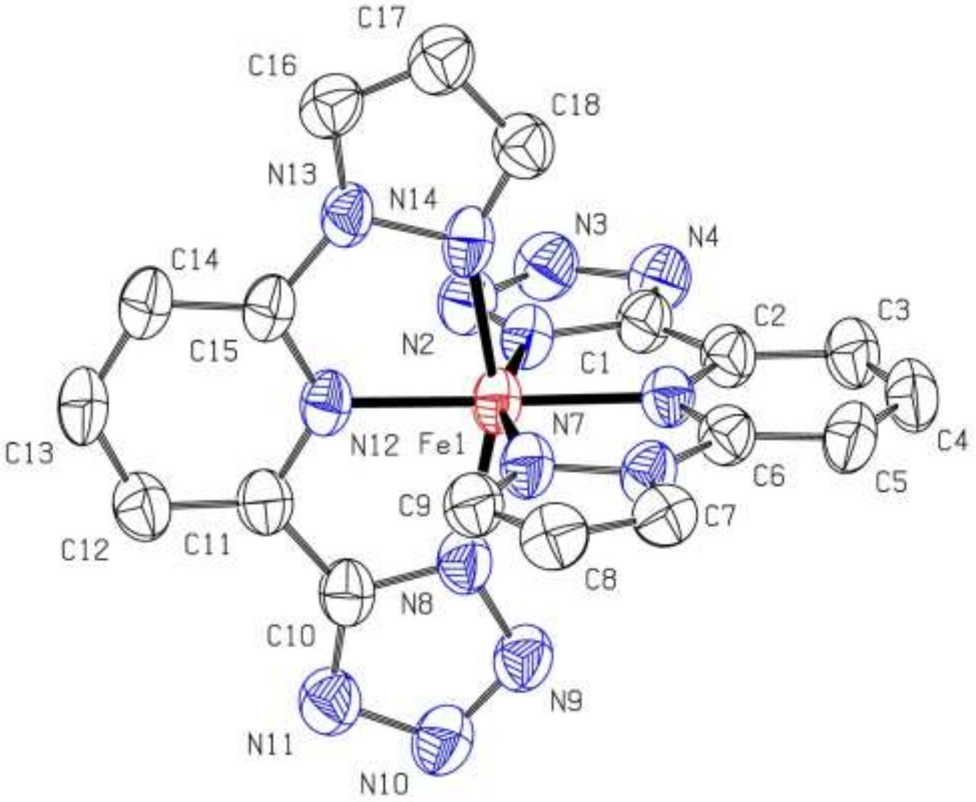

Figure S1: Molecular of **1** (H atoms and crystal solvent molecules omitted)

Empirical formula	$C_{19.25}H_{17}FeN_{14}O_{1.25}$
M [g mol^{-1}]	520.32
Crystal colour	yellow
T [K]	180(2) K
λ [Å]	0.71073
Crystal system	monoclinic
space group	*C2/c*
a [pm]	2389.6(6)
b [pm]	1492.59(19)
c [pm]	1561.9(5)

β [°]	129.108(15)
V [Å^3]	4322.5(18)
Z	8
$\rho_{\text{calcd.}}$ [g cm^{-3}]	1.599
μ(Mo-K_α) [mm^{-1}]	0.747
F(000)	2132
Crystal size [mm]	0.27 x 0.12 x 0.11
θ range for data collection [°]	2.20 – 24.70
Limiting indices	-27<=h<=27, -17<=k<=15, -18<=l<=17
Reflections collected / unique	9918 / 3549
R(int) =	0.0828
Reflections with I>2σ(I)	1861
Completeness to θ = 24.70	96.4 %
Absorption correction	none
Refinement method	Full-matrix least-squares on F^2
Data / restraints / parameters	3549 / 5 / 328
Extinction coefficient	0.00078(16)
Largest diff. peak and hole	0.582 and -0.383 e.A^{-3}
Final *R* indices [$I>2\sigma(I)$][a]	R_1 = 0.0495, wR_2 = 0.1175
R indices (all data)[a]	R_1 = 0.1035, wR_2 = 0.1342
GoF on F_2	0.847

[a] $R_1 = \Sigma(F_o – F_c)/\Sigma(F_o)$; $wR_2 = \{\Sigma[w(F_o{}^2 – Fc{}^2)^2]/\Sigma[w(F_c{}^2)^2]\}^{1/2}$.

Table S1. Crystal data for compound **1** [Fe($C_9H_6N_7$)$_2$].

Fe(1)-N(5)	191.6(3)
Fe(1)-N(12)	191.8(3)
Fe(1)-N(7)	194.9(4)
Fe(1)-N(14)	195.9(4)
Fe(1)-N(1)	196.8(4)
Fe(1)-N(8)	197.1(4)
N(1)-N(2)	133.5(5)
N(1)-C(1)	135.8(5)
N(2)-N(3)	133.9(5)
N(3)-N(4)	136.9(5)
N(4)-C(1)	132.4(6)
N(5)-C(6)	132.2(6)
N(5)-C(2)	135.3(6)
N(6)-C(7)	135.5(6)
N(6)-N(7)	139.9(5)
N(6)-C(6)	141.4(6)
N(7)-C(9)	132.9(6)
N(8)-N(9)	135.5(5)
N(8)-C(10)	136.4(5)

N(9)-N(10)	132.4(5)
N(10)-N(11)	136.2(5)
N(11)-C(10)	132.4(6)
N(12)-C(15)	132.1(6)
N(12)-C(11)	135.2(6)
N(13)-C(16)	135.4(6)
N(13)-N(14)	139.7(4)
N(13)-C(15)	140.5(6)
N(14)-C(18)	133.7(6)
C(1)-C(2)	145.1(7)
C(2)-C(3)	139.4(5)
C(3)-C(4)	138.3(7)
C(4)-C(5)	138.5(7)
C(5)-C(6)	138.7(5)
C(7)-C(8)	135.5(6)
C(8)-C(9)	137.4(7)
C(10)-C(11)	144.9(6)
C(11)-C(12)	138.8(5)
C(12)-C(13)	137.9(7)
C(13)-C(14)	139.6(7)
C(14)-C(15)	139.3(5)
C(16)-C(17)	136.2(6)
C(17)-C(18)	140.3(6)
O(1)-C(19)	133.1(15)
O(2)-C(20)	159(4)
O(3)-C(21)	152(2)
N(5)-Fe(1)-N(12)	177.48(16)
N(5)-Fe(1)-N(7)	79.98(15)
N(12)-Fe(1)-N(7)	98.19(14)
N(5)-Fe(1)-N(14)	97.88(15)
N(12)-Fe(1)-N(14)	80.39(16)
N(7)-Fe(1)-N(14)	91.14(16)
N(5)-Fe(1)-N(1)	80.08(15)
N(12)-Fe(1)-N(1)	101.77(15)
N(7)-Fe(1)-N(1)	160.04(14)
N(14)-Fe(1)-N(1)	92.34(16)
N(5)-Fe(1)-N(8)	102.26(14)
N(12)-Fe(1)-N(8)	79.45(15)
N(7)-Fe(1)-N(8)	91.27(16)
N(14)-Fe(1)-N(8)	159.83(14)
N(1)-Fe(1)-N(8)	92.20(17)

N(2)-N(1)-C(1)	105.7(4)
N(2)-N(1)-Fe(1)	139.9(3)
C(1)-N(1)-Fe(1)	114.4(3)
N(1)-N(2)-N(3)	108.5(3)
N(2)-N(3)-N(4)	109.6(4)
C(1)-N(4)-N(3)	104.4(3)
C(6)-N(5)-C(2)	120.0(4)
C(6)-N(5)-Fe(1)	120.0(3)
C(2)-N(5)-Fe(1)	120.0(3)
C(7)-N(6)-N(7)	111.5(3)
C(7)-N(6)-C(6)	133.8(4)
N(7)-N(6)-C(6)	114.7(4)
C(9)-N(7)-N(6)	103.2(4)
C(9)-N(7)-Fe(1)	143.0(3)
N(6)-N(7)-Fe(1)	113.8(3)
N(9)-N(8)-C(10)	105.0(4)
N(9)-N(8)-Fe(1)	140.1(3)
C(10)-N(8)-Fe(1)	114.9(3)
N(10)-N(9)-N(8)	107.6(3)
N(9)-N(10)-N(11)	111.5(4)
C(10)-N(11)-N(10)	103.5(4)
C(15)-N(12)-C(11)	120.1(3)
C(15)-N(12)-Fe(1)	119.2(3)
C(11)-N(12)-Fe(1)	120.6(3)
C(16)-N(13)-N(14)	110.7(4)
C(16)-N(13)-C(15)	133.5(3)
N(14)-N(13)-C(15)	115.3(4)
C(18)-N(14)-N(13)	104.2(4)
C(18)-N(14)-Fe(1)	143.0(3)
N(13)-N(14)-Fe(1)	112.7(3)
N(4)-C(1)-N(1)	111.9(4)
N(4)-C(1)-C(2)	132.2(4)
N(1)-C(1)-C(2)	115.9(4)
N(5)-C(2)-C(3)	119.8(4)
N(5)-C(2)-C(1)	109.6(3)
C(3)-C(2)-C(1)	130.5(4)
C(4)-C(3)-C(2)	119.1(4)
C(3)-C(4)-C(5)	121.0(4)
C(4)-C(5)-C(6)	116.2(5)
N(5)-C(6)-C(5)	123.9(4)
N(5)-C(6)-N(6)	111.5(4)
C(5)-C(6)-N(6)	124.6(5)

N(6)-C(7)-C(8)	106.0(4)
C(7)-C(8)-C(9)	107.4(5)
N(7)-C(9)-C(8)	112.0(4)
N(11)-C(10)-N(8)	112.4(4)
N(11)-C(10)-C(11)	132.2(4)
N(8)-C(10)-C(11)	115.3(5)
N(12)-C(11)-C(12)	120.8(4)
N(12)-C(11)-C(10)	109.5(4)
C(12)-C(11)-C(10)	129.7(5)
C(13)-C(12)-C(11)	118.5(5)
C(12)-C(13)-C(14)	121.2(4)
C(15)-C(14)-C(13)	116.1(5)
N(12)-C(15)-C(14)	123.4(5)
N(12)-C(15)-N(13)	112.1(3)
C(14)-C(15)-N(13)	124.5(4)
N(13)-C(16)-C(17)	107.8(4)
C(16)-C(17)-C(18)	105.8(5)
N(14)-C(18)-C(17)	111.4(4)

Table S2. Bond lengths [Å] and angles [°] for **1**.

4. Intermolecular Interactions in the crystal lattice of **1**

A detailed inspection of the crystal lattice of **1** shows two types of intermolecular interactions of neighbouring complexes: A) a π-stacking between two pyrazolyl units, and B) an edge-to-face π-stacking between a pyrazolyl ring and a tetrazolyl ring

A) π-stacking between the pyrazolyl units of neighbouring complexes was found. The distances of the C atoms (C16, C17, and C18) of one pyrazolyl ring to the pyrazolyl ring plane (N6-N7-C7-C8-C9) of the neighbouring complex are 3.27, 3.28, and 3.31 Å respectively (Figure S2).

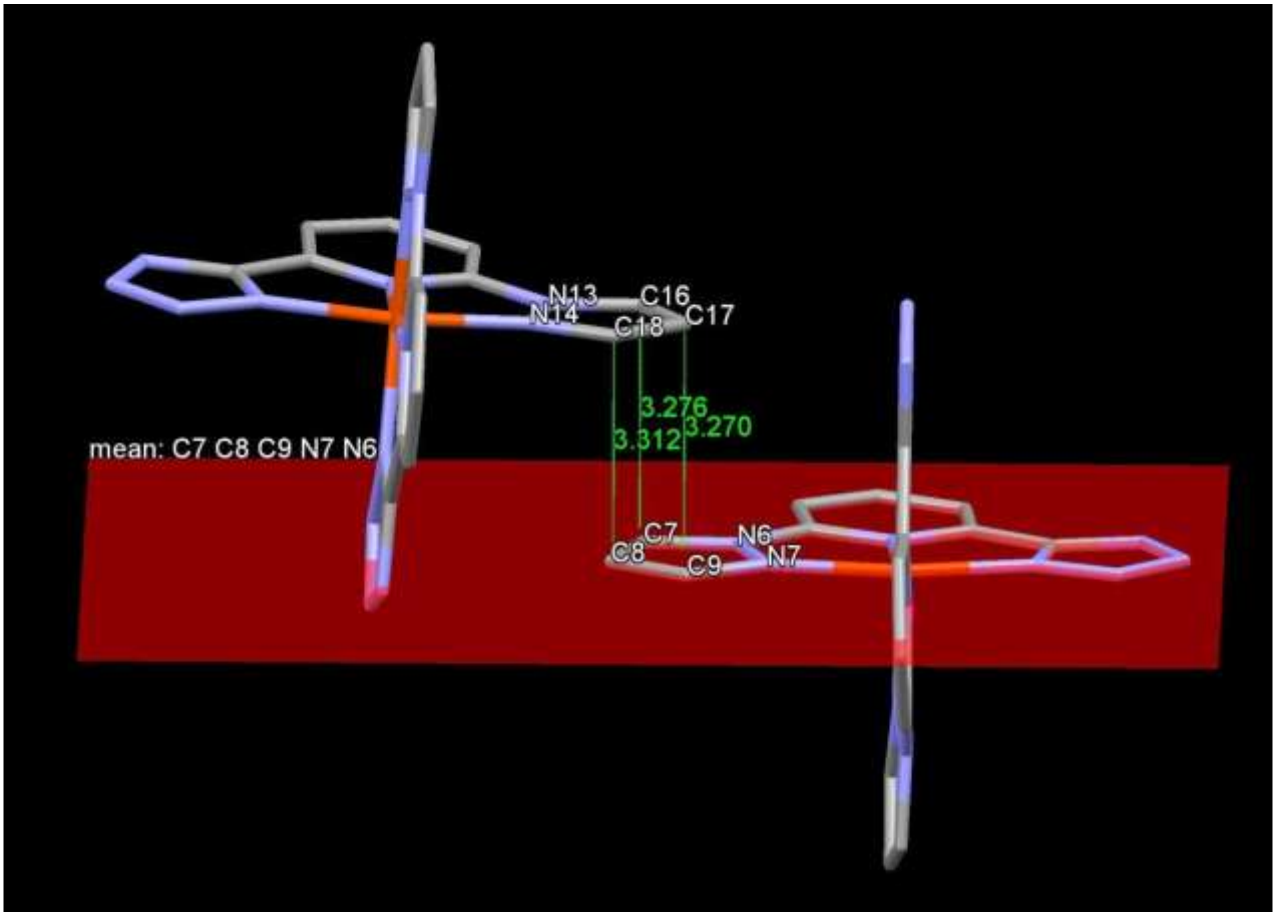

Figure S2: π-stacking between the pyrazolyl units of neighbouring complexes in the crystal lattice of **1**; the green colour code indicates the distances of the C atoms C16, C17, and C18 of one pyrazolyl ring to the pyrazolyl ring plane of (N6-N7-C7-C8-C9) which are 3.27, 3.28, and 3.31 Å.

Furthermore, an edge-to-face π-stacking between the (N6-N7-C7-C8-C9) pyrazolyl ring and the (N1-N2-N3-N4-C1) tetrazolyl ring of the neighbouring complex was found. The angle between the planes of these two rings is about 84° (Figure S3). While the distance of the centroid of the (N6-N7-C7-C8-C9) pyrazolyl ring to the tetrazolyl (N1-N2-N3-N4-C1) ring plane is about 4.53 Å (Figure S4).

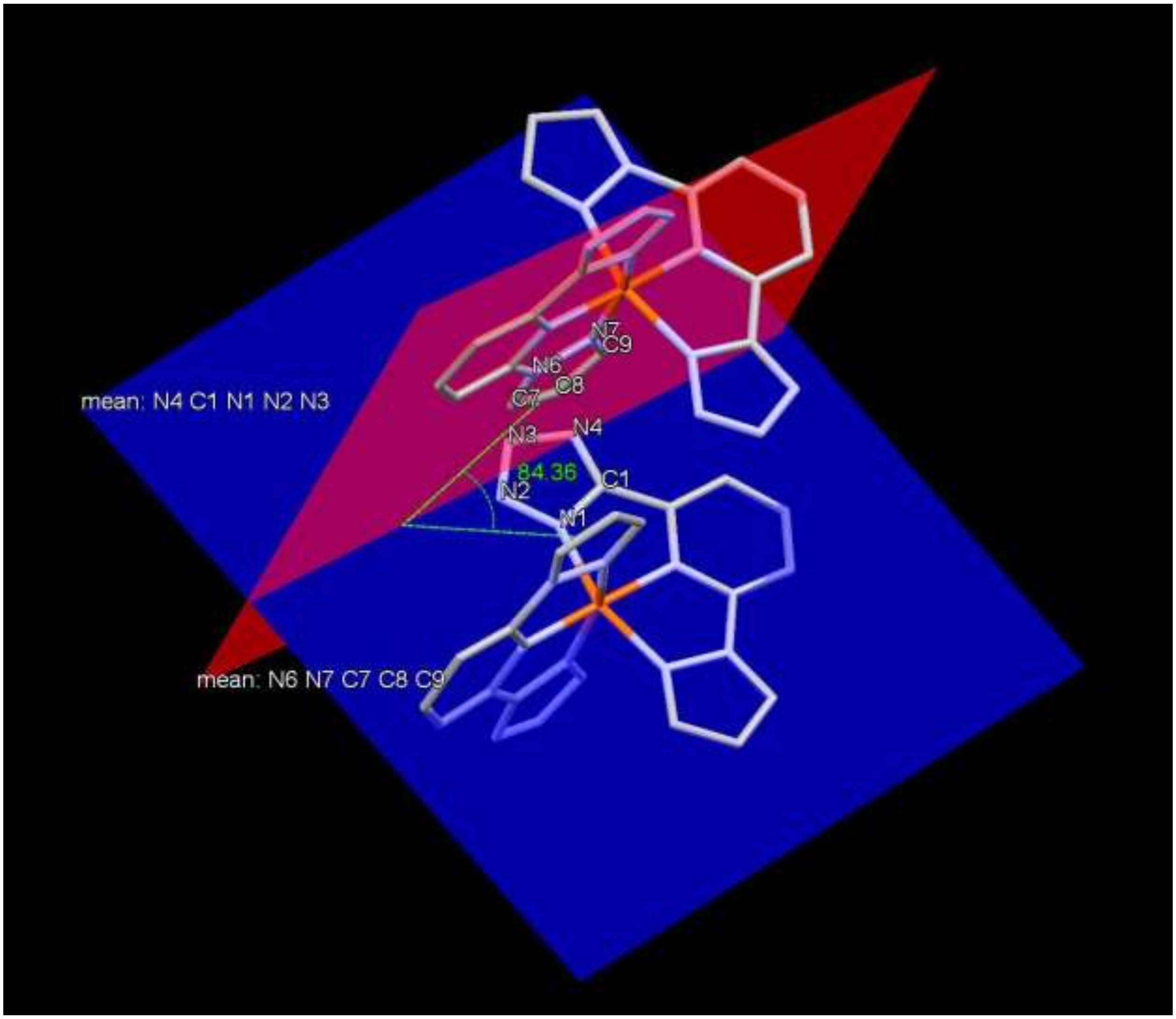

Figure S3: Edge-to-face π-stacking between the (N6-N7-C7-C8-C9) pyrazolyl ring and the (N1-N2-N3-N4-C1) tetrazolyl ring of neighbouring complexes in the crystal lattice of **1**. The angle between the two ring planes is about 84°.

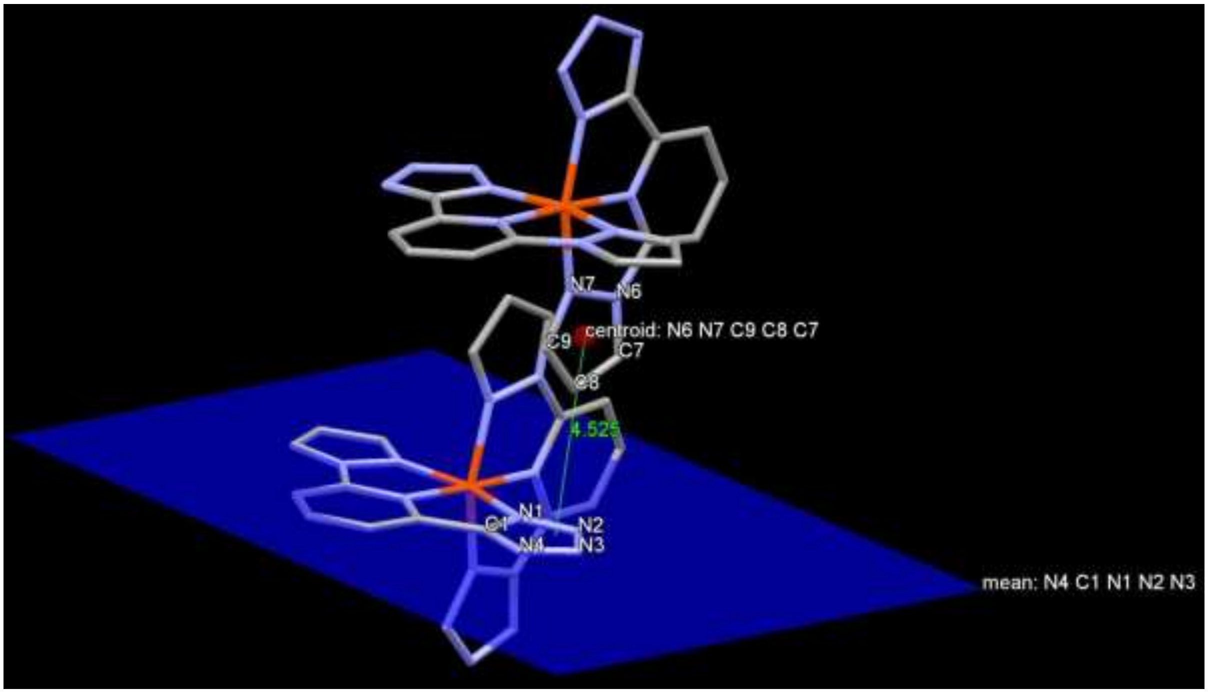

Figure S4: Illustrates the edge-to-face π-stacking between the (N6-N7-C7-C8-C9) pyrazolyl ring and the (N1-N2-N3-N4-C1) tetrazolyl ring of neighbouring complexes in the crystal lattice of **1**. The green colour code shows the distance of about 4.53 Å of the centroid of the (N6-N7-C7-C8-C9) atoms of the pyrazolyl ring to the tetrazolyl (N1-N2-N3-N4-C1) ring plane.

5. XAS experiments

Via X-ray absorption spectroscopy (XAS) the spin transition was studied element-specifically. The measurements were performed at the beamline UE46-PGM1 at BESSY II – Helmholtz-Zentrum Berlin. Before inserting the sample into the UHV chamber, we fixed the powder of complex **1** on the sample holder by the help of an UHV-suitable adhesive tape. We estimated the layer thickness to 150-200 μm by eye. Only the surface of the sample contributes to the XAS measurement that is why such estimation is justified. The pressure during the measurements was 10^{-10} mbar. With circular polarized X-rays in magnetic fields up to B=6 T in the UE46-PGM1 high-field chamber we were able to measure the X-ray magnetic circular dichroism (XMCD). Since organic samples can be affected easily by high intense X-rays and photoelectrons, we carried out the measurements with a highly reduced X-ray intensity and scanned the sample position regularly that was hit by the photons. By analysing and comparing successively recorded spectra we can rule out that the molecules are affected by the radiation.

6. References

1. X. Deng, A. Roessler, I. Brdar, R. Faessler, J. Wu, Z. S. Sales, and N. S. Mani, *J. Org. Chem.*, 2011, **76**, 8262–8269.
2. F. W. Joachim Demnitz and M. B. D’heni, *Org. Prep. Proced. Int.*, 1998, **30**, 467–469.
3. O. Kahn, *Molecular magnetism*, VCH, New York, NY, 1993.
4. G. M. Sheldrick, *Acta Crystallogr. A*, 1990, **46**, 467–473.